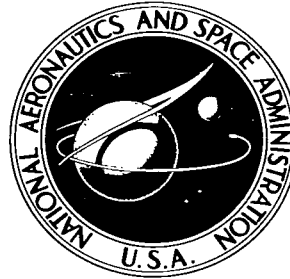


NASA TECHNICAL NOTE



NASA TN D-3853

0.1

NASA TN D-3853

LOAN COPY RETURN TO  
AFWL (WLF) 11  
KIRTLAND AFB, N.M.

0130657



# LOW SUBSONIC STATIC AND DYNAMIC STABILITY CHARACTERISTICS OF TWO BLUNT $120^\circ$ CONE CONFIGURATIONS

*by Richard J. Bendura*  
*Langley Research Center*  
*Langley Station, Hampton, Va.*





LOW SUBSONIC STATIC AND DYNAMIC STABILITY CHARACTERISTICS  
OF TWO BLUNT 120° CONE CONFIGURATIONS

By Richard J. Bendura

Langley Research Center  
Langley Station, Hampton, Va.

NATIONAL AERONAUTICS AND SPACE ADMINISTRATION

---

For sale by the Clearinghouse for Federal Scientific and Technical Information  
Springfield, Virginia 22151 - Price \$1.00

# LOW SUBSONIC STATIC AND DYNAMIC STABILITY CHARACTERISTICS OF TWO BLUNT 120° CONE CONFIGURATIONS

By Richard J. Bendura  
Langley Research Center

## SUMMARY

Static and dynamic stability characteristics of two 120° total angle cone configurations have been experimentally determined. One configuration had a flat base and one configuration had a conical base. Both configurations had a nose-radius—base-diameter ratio of 1/8. Two models of each configuration were tested: one model with the center of gravity in the vicinity of the nose and one model with the center of gravity near the maximum body diameter.

The investigation was conducted with the flat-base configuration at a Mach number of 0.052 and Reynolds number of  $0.58 \times 10^6$  (based on maximum body diameter) and with the conical-base configuration at a Mach number of 0.057 and Reynolds number of  $0.63 \times 10^6$ . Both configurations were statically and dynamically stable for all center-of-gravity locations forward of the maximum base diameter. The conical afterbody had no significant effect on either the static stability or the dynamic stability.

## INTRODUCTION

Recently, large angle blunted cones have been seriously considered as configurations for entry into low-density planetary atmospheres. This is due primarily to the low ballistic coefficient for such bodies. Several flight programs currently proposed are utilizing a blunt 120° total angle cone as a payload. Since these programs include velocities ranging from planetary entry to low subsonic, aerodynamic characteristics for this configuration are needed for all Mach number ranges.

This investigation was conducted to provide experimental values of static stability and dynamic stability for a blunt 120° total angle cone at low subsonic velocities. In order to determine experimentally the dynamic stability characteristics of a body by the natural decay method, it is advantageous that the body be free of any physical restraints tending to retard its natural motion during the test. The Langley spin tunnel, in which these tests were performed, is uniquely suited to meet this condition. The method used to analyze the data obtained in this investigation is similar to that presented in

reference 1. The results of a similar investigation dealing with several blunt bodies of revolution and conducted in the same facility may be found in reference 2.

### SYMBOLS

Dimensions are given in the International System of Units (SI) with the U.S. Customary Units in parentheses. (See ref. 3.)

A maximum cross-sectional area of body, meters<sup>2</sup> (feet<sup>2</sup>)

$C_D$  drag coefficient,  $\frac{\text{Total drag}}{q_\infty A}$

$C_m$  pitching-moment coefficient,  $\frac{\text{Pitching moment}}{q_\infty A d}$

$C_{m_q} = \frac{\partial C_m}{\partial (qd/2V)}$ , per radian

$\overline{C_{m_q}}$  dynamic stability derivative,  $C_{m_q} + C_{m_{\dot{\alpha}}}$ , per radian

$C_{m_\alpha}$  pitching-moment-curve slope,  $\frac{\partial C_m}{\partial \alpha}$ , per radian

$C_{m_{\dot{\alpha}}} = \frac{\partial C_m}{\partial (\dot{\alpha}d/2V)}$ , per radian

$C_N$  normal-force coefficient,  $\frac{\text{Normal force}}{q_\infty A}$

$C_{N_q} = \frac{\partial C_N}{\partial (qd/2V)}$ , per radian

$C_{N_\alpha}$  normal-force-curve slope,  $\frac{\partial C_N}{\partial \alpha}$ , per radian

d maximum body diameter, meters (feet)

I moment of inertia about pitch axis, kilograms-meters<sup>2</sup> (slugs-feet<sup>2</sup>)

K radius of gyration,  $(I/m)^{1/2}$ , meters (feet)

m mass of model, kilograms (slugs)

$q$	pitching velocity, radians/second
$q_{\infty}$	free-stream dynamic pressure, newtons/meters <sup>2</sup> (pounds force/foot <sup>2</sup> )
$r$	nose radius, centimeters (inches)
$T_{1/2}$	time to damp to half-amplitude, seconds
$V$	free-stream velocity, meters/second (feet/second)
$W$	weight of model, kilograms (pounds mass)
$x_{cg}$	axial distance to center of gravity, measured aft from nose, centimeters (inches)
$x_{cp}$	axial distance to center of pressure, measured aft from nose, centimeters (inches)
$\alpha$	angle of attack, degrees
$\dot{\alpha}$	time rate of change of angle of attack, radians/second
$\alpha_p$	peak angle of attack during model oscillation, degrees
$\lambda$	damping parameter, $-\frac{\ln 2}{T_{1/2}}$
$\rho$	atmospheric density, kilograms/meter <sup>3</sup> (slugs/foot <sup>3</sup> )
$\omega$	frequency of oscillation, radians/second
Subscript:	
0	refers to center of gravity at nose

### MODELS

Two lightweight foam models of two 120° total angle cone configurations were used in the investigation. One configuration had a flat base and one configuration had a conical base. All four cone models had a bluntness ratio  $r/d$  of 1/8 and a maximum body

diameter of 48.3 cm (19.0 in.). Steel weights were inserted in the models during construction to obtain different center-of-gravity locations. The center of gravity of one model of each configuration was near the nose and that of the other model was in the vicinity of the maximum body diameter. These locations would bracket the center of gravity for most flight configurations. Sketches of the configurations and the center-of-gravity location for each model are shown in figure 1. Photographs of the flat-base configuration and the conical-base configuration are presented in figures 2 and 3, respectively. Physical properties of the models are listed in table 1.

TABLE 1.- PHYSICAL PROPERTIES

	Model 1	Model 2	Model 3	Model 4
W, kg (lbm) . . . . .	3.40 (7.5)	3.40 (7.5)	3.86 (8.5)	3.86 (8.5)
$x_{cg}/d$ . . . . .	0.101	0.227	0.119	0.273
I, kg-m <sup>2</sup> (slugs-ft <sup>2</sup> ) . . .	0.018 (0.013)	0.011 (0.008)	0.023 (0.017)	0.018 (0.013)

#### FACILITY AND TEST PROCEDURE

The tests were conducted in the Langley spin tunnel. A unique feature of this tunnel is that the air flows in a vertical direction and thereby free-flight investigations can be initiated from a state of equilibrium. Further information concerning this facility may be obtained in reference 4.

The flat-base models were tested at a Mach number of 0.052 and Reynolds number of  $0.58 \times 10^6$  based on maximum body diameter. The conical-base models were tested at a Mach number of 0.057 and Reynolds number of  $0.63 \times 10^6$ .

After the free-stream velocity approached the desired value, the model was inserted into the tunnel and allowed to reach approximate equilibrium conditions. (The free-stream velocity was obtained from a calibration chart in which air velocity at the center of the tunnel is compared with the angular speed of the tunnel fan.) The model was then disturbed and the resulting motions were recorded by means of a 16-mm motion-picture camera at a film speed of 60 frames per second. The model was disturbed in such a manner that the resulting oscillations took place in a vertical plane normal to the optical axis of the camera. Data were discarded from tests in which observable deviations from this condition occurred. The camera also recorded elapsed time and air velocity during the test.

Horizontal lines were painted around the interior of the tunnel in increments of  $10^0$  measured from the optical axis of the camera. These lines appeared in the motion

pictures taken during the tests and were used to determine any displacement of the model from the horizontal plane of the camera. Data obtained from tests in which large displacements (exceeding  $12^\circ$ ) occurred were not used.

### EXPERIMENTAL ACCURACY

Values of free-stream velocity are estimated to be accurate within  $\pm 0.3$  m/sec ( $\pm 1$  ft/sec). This value gives an accuracy variation in  $C_D$  of approximately  $\pm 0.03$ . Angle of attack could be read to an accuracy of  $\pm 1^\circ$ . The accuracy in  $C_{m_\alpha}$  was estimated from a first-order analysis considering inaccuracies in determining free-stream dynamic pressure and oscillation frequency.

By using the extreme values of  $C_{m_\alpha}$  given by the foregoing error analysis, the ranges of  $C_{N_\alpha}$  and  $x_{cp}/d$  were determined for each configuration. It is expected that the inaccuracy of these two parameters would have been smaller if models with significantly larger center-of-gravity variations could have been accommodated. However, because of physical limitations of the configurations, center-of-gravity variations between the models were small.

The inaccuracies of  $\lambda$  and  $C_{N_\alpha}$  were used in determining inaccuracies for the dynamic stability parameters  $\overline{C_{mq}}$  and  $C_{Nq}$ . The estimated accuracy of the aerodynamic parameters determined in this investigation is given in table 2.

TABLE 2.- ESTIMATED ACCURACY OF AERODYNAMIC PARAMETERS

	Model 1	Model 2	Model 3	Model 4
$C_D$ . . . . .	$\pm 0.03$	$\pm 0.03$	$\pm 0.03$	$\pm 0.03$
$C_{m_\alpha}$ . . . . .	$\pm 0.01$	$\pm 0.01$	$\pm 0.01$	$\pm 0.01$
$C_{N_\alpha}$ . . . . .	+0.17 -0.07	+0.17 -0.07	+0.13 -0.14	+0.13 -0.14
$x_{cg}/d$ . . . . .	+0.18 -0.08	+0.18 -0.08	+0.34 -0.14	+0.34 -0.14
$\overline{C_{mq}}$ . . . . .	$\pm 0.07$	$\pm 0.03$	$\pm 0.05$	$\pm 0.02$
$C_{Nq}$ . . . . .	$\pm 0.16$	$\pm 0.10$	$\pm 0.16$	$\pm 0.18$

## DATA REDUCTION

The recorded equilibrium free-stream velocities were 17.7 m/sec (58 ft/sec) for the flat-base configuration and 19.2 m/sec (63 ft/sec) for the conical-base configuration. The drag coefficients were then calculated and are 0.95 for the flat-base configuration and 0.92 for the conical-base configuration.

The tests meeting the aforementioned angular-displacement and planar-motion requirements were selected for further analysis. The time history of angle of attack was measured directly from the motion-picture film. The variation in  $\alpha$  due to horizontal translations affecting the velocity vector was neglected.

Curves were faired encompassing the peaks of the  $\alpha$  oscillation. A line to indicate the trim angle of attack was then drawn midway between the enveloping curves and all measurements were referenced to this line. Figure 4 presents the raw data of a selected test, envelope fairing, and trim line. The presence of a trim angle of attack other than zero was caused by small center-of-gravity offsets and minor model fabrication asymmetries. The maximum angle of attack  $\alpha_p$  and frequency of oscillation  $\omega$  for each peak were measured. Reference 1 contains the basic method and equations for the determination of the static and dynamic stability characteristics of a model by using the foregoing data. Linear aerodynamic characteristics were assumed for the angle-of-attack range through which the configurations were tested. Prior publications, such as reference 5 indicate that this is a reasonable assumption. In addition, for the equations that follow,  $\overline{C_{mq}}$  is assumed to be equal to  $C_{mq}$ .

To minimize errors present in any individual test, values of  $\alpha_p$  and  $\omega$  obtained from a minimum of four tests for each model were combined. These data were then faired to arrive at average angle-of-attack envelopes and frequencies for each model, as shown in figure 5.

The equation for aerodynamic frequency of the motion about trim for zero spin is

$$\omega^2 = \frac{1}{4} \left[ -P - (Q + R)^2 \right]$$

where

$$P = \frac{4C_{m\alpha}q_\infty Ad}{I}$$

$$Q = \frac{C_{N\alpha}q_\infty A}{mV}$$

$$R = \frac{\overline{C_{mq}} q_{\infty} Ad^2}{2VI}$$

For this investigation

$$P \gg (Q + R)^2$$

Therefore  $C_{m\alpha}$  may be expressed by

$$C_{m\alpha} = - \frac{\omega^2 I}{q_{\infty} Ad}$$

By using the average values of  $\omega$  from figures 5(a) to 5(d) in this equation, the value of  $C_{m\alpha}$  for each model was determined.

Having calculated  $C_{m\alpha}$  about two center-of-gravity locations, the variation of  $C_{m\alpha}$  with  $x_{cg}$  was then determined for each configuration as shown in figure 6. In addition,  $C_{N\alpha}$  and  $x_{cp}/d$  were calculated and are as follows:

Configuration	$C_{N\alpha}$	$x_{cp}/d$
Flat base . . . . .	0.48	0.49
Conical base . . . . .	0.31	0.67

Reference 1 gives the dynamic stability parameter for motion about trim with constant flight-path angle as

$$\overline{C_{mq}} = 2 \left( \frac{K}{d} \right)^2 \left( \frac{4m}{\rho AV} \lambda + C_{N\alpha} \right)$$

where

$$\lambda = - \frac{\ln 2}{T_{1/2}}$$

Values of  $T_{1/2}$  were obtained directly from the variation of  $\alpha_p$  with time (fig. 5) for each model. Average values of  $\lambda$  were then used in determining  $\overline{C_{mq}}$ . Figure 7 shows the variation of  $\overline{C_{mq}}$  with  $x_{cg}/d$  for both configurations.

In order to obtain the faired curve through the data points, the axis transfer equation (from ref. 6)

$$\overline{C_{m\alpha}} = (C_{m\alpha})_0 - 2 \frac{x_{cg}}{d} (C_{m\alpha})_0 + \frac{x_{cg}}{d} (C_{Nq})_0 - 2 \left( \frac{x_{cg}}{d} \right)^2 C_{N\alpha}$$

was used to yield two equations with two unknowns  $\left( (C_{m\alpha})_0 \text{ and } (C_{Nq})_0 \right)$  which were determined by simultaneous solution.

The effect of  $x_{cg}/d$  on  $C_{Nq}$  was calculated by use of

$$C_{Nq} = (C_{Nq})_0 - 2 \left( \frac{x_{cg}}{d} \right) C_{N\alpha}$$

(from ref. 6) and is shown in figure 8.

## RESULTS AND DISCUSSION

The primary data obtained from this investigation are presented in figures 6 and 7. Two values of  $C_{m\alpha}$  and  $\overline{C_{m\alpha}}$  for each configuration were determined directly from experimental data, and symbols mark these points at the appropriate center-of-gravity locations. In addition, the accuracy range is shown for each experimentally determined parameter. Considering the possible variation in data within the accuracy ranges determined, both configurations are statically and dynamically stable for all center-of-gravity locations forward of the maximum body diameter.

The test results indicate that, for center-of-gravity locations in the vicinity of the nose, the conical-base configuration is more dynamically stable and the flat-base configuration is more statically stable and that, for center-of-gravity locations in the vicinity of the maximum diameter, the conical-base configuration is more statically stable and the flat-base configuration is more dynamically stable.

However, for most practical spacecraft design, the center of gravity would lie between, rather than at, the extreme locations studied. Therefore, within the accuracies of this investigation, the afterbody had no significant effect on either the static stability or the dynamic stability.

Because of the inaccuracies present in determining the parameters, values of  $C_{N\alpha}$ ,  $x_{cp}/d$ , and  $C_{Nq}$  for the two configurations are presented only as a matter of interest.

## CONCLUDING REMARKS

Static and dynamic stability characteristics of two blunted  $120^\circ$  total angle cone configurations (one with a flat base and one with a conical base) were determined for low subsonic conditions. Both configurations had a nose-radius—base-diameter ratio of  $1/8$  and were statically and dynamically stable for center-of-gravity locations forward of the maximum body diameter. The conical afterbody had no significant effect on either the static stability or the dynamic stability for this investigation.

Langley Research Center,  
National Aeronautics and Space Administration,  
Langley Station, Hampton, Va., November 14, 1966,  
124-07-03-05-23.

## REFERENCES

1. Nelson, Robert L.: The Motions of Rolling Symmetrical Missiles Referred to a Body-Axis System. NACA TN 3737, 1956.
2. Marte, Jack E.; and Weaver, Robert W.: Low Subsonic Dynamic-Stability Investigation of Several Planetary-Entry Configurations in a Vertical Wind Tunnel (Part I). Tech. Rept. No. 32-743 (Contract No. NAS 7-100), Jet Propulsion Lab., California Inst. Technol., May 1, 1965.
3. Mechtly, E. A.: The International System of Units – Physical Constants and Conversion Factors. NASA SP-7012, 1964.
4. Neihouse, Anshal I.; Klinar, Walter J.; and Scher, Stanley H.: Status of Spin Research for Recent Airplane Designs. NASA TR R-57, 1960. (Supersedes NACA RM L57F12.)
5. Anon.: Comparative Studies of Conceptual Design and Qualification Procedures for a Mars Probe/Lander. Volume V: Subsystem and Technical Analyses – Book 2: Aeromechanics and Thermal Control. AVSSD-0006-66-RR (Contract NAS 1-5224), AVCO Corp., May 11, 1966.
6. Fisher, Lewis R.: Equations and Charts for Determining the Hypersonic Stability Derivatives of Combinations of Cone Frustums Computed by Newtonian Impact Theory. NASA TN D-149, 1959.

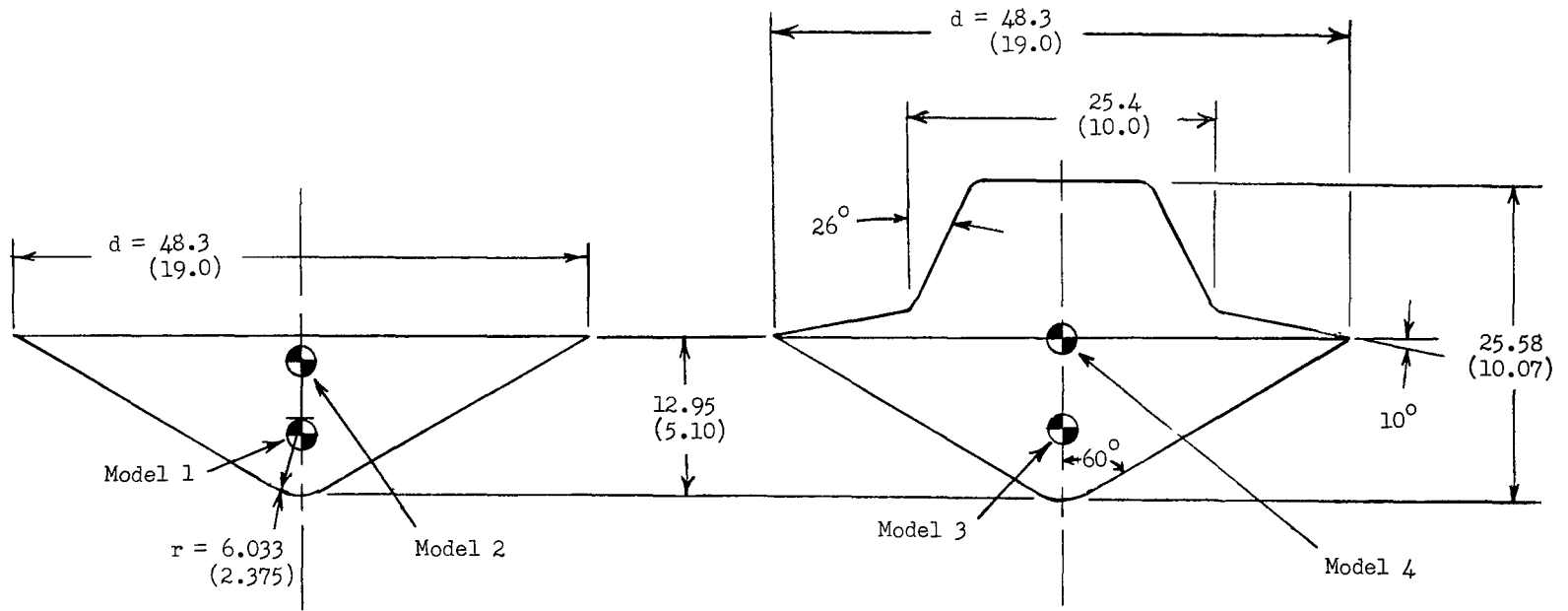


Figure 1.- Sketches of configurations. All dimensions are in centimeters (inches).

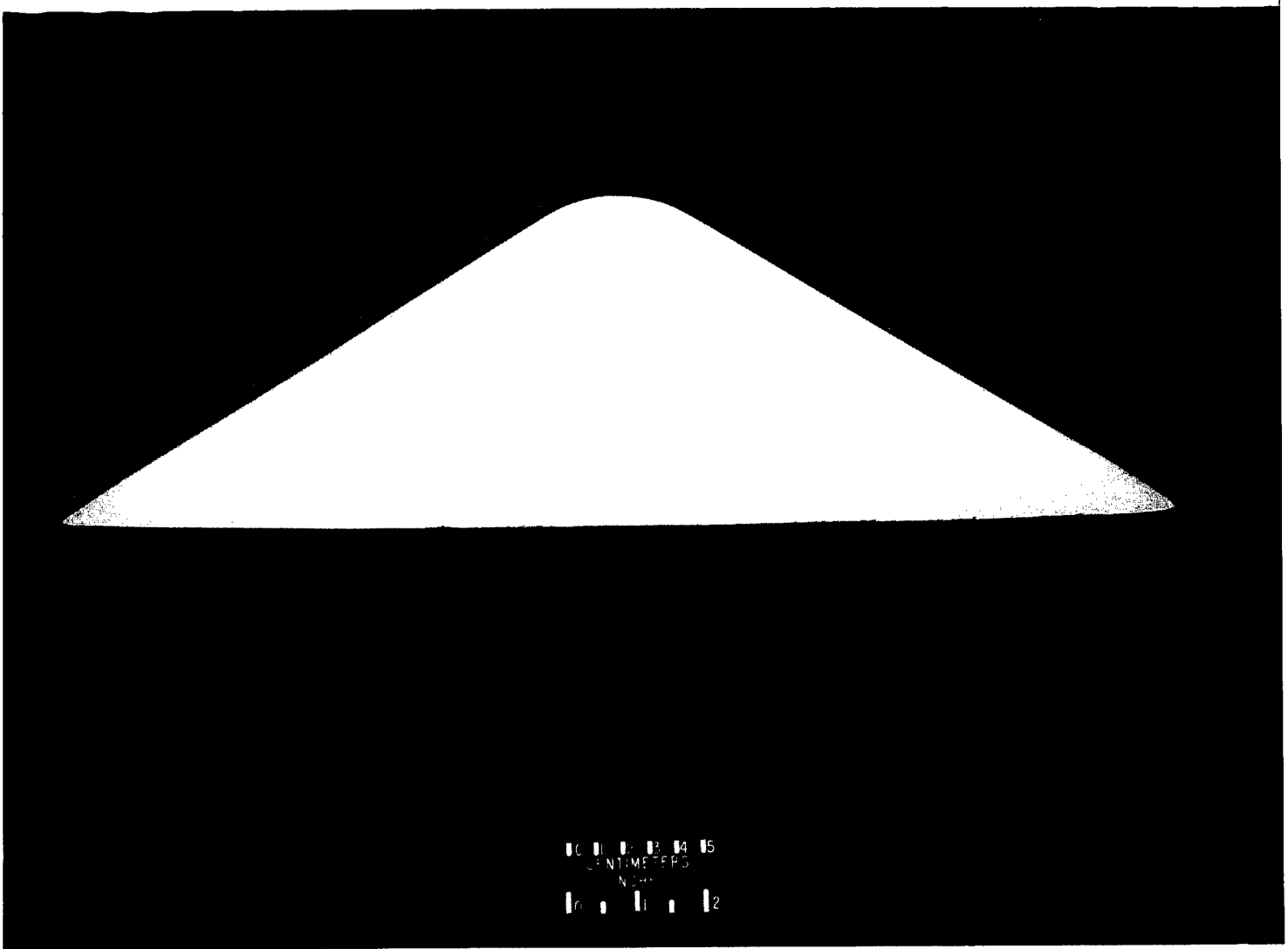


Figure 2.- Flat-base configuration.

L-66-7188

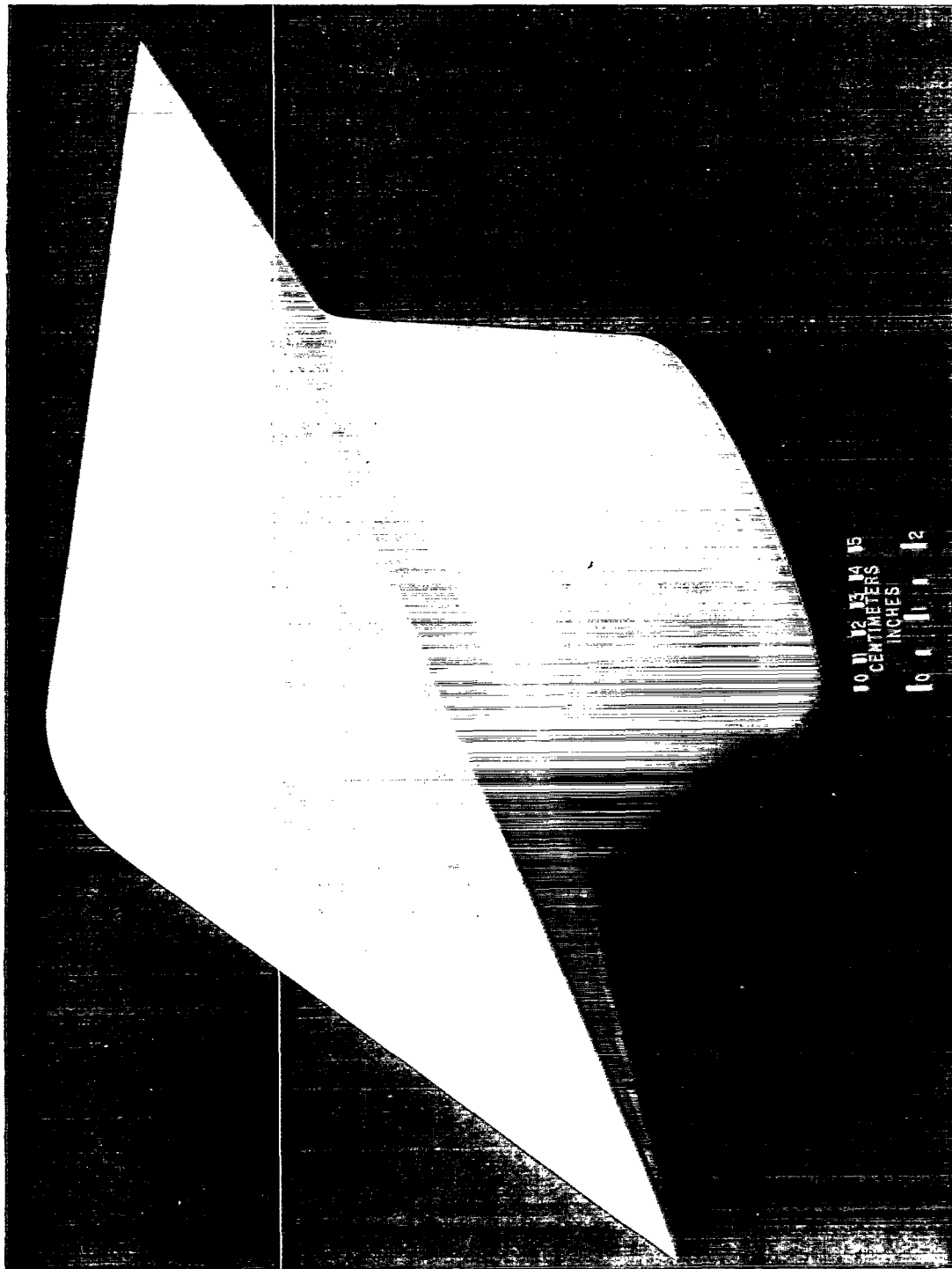


Figure 3.- Conical-base configuration.

L-65-9405

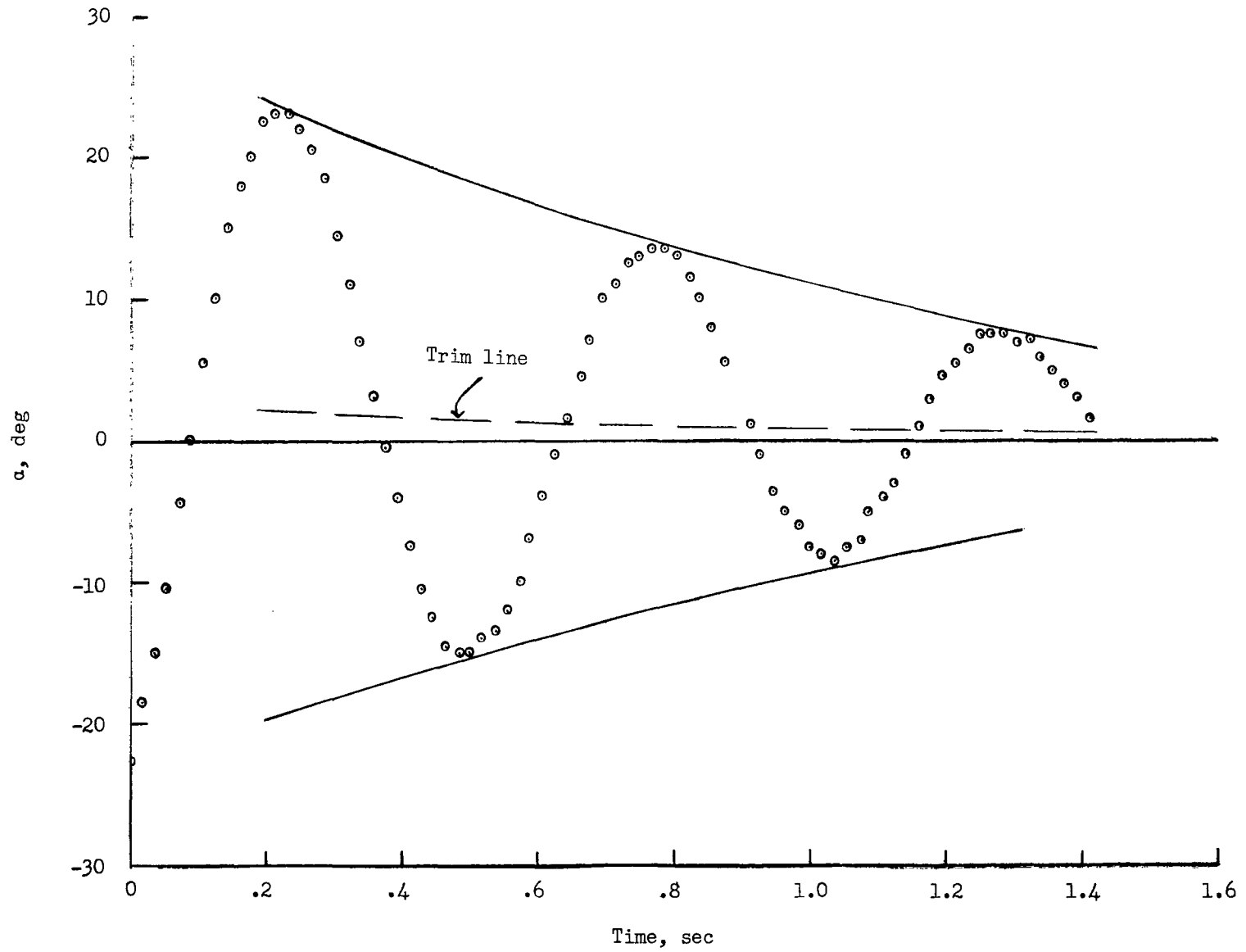
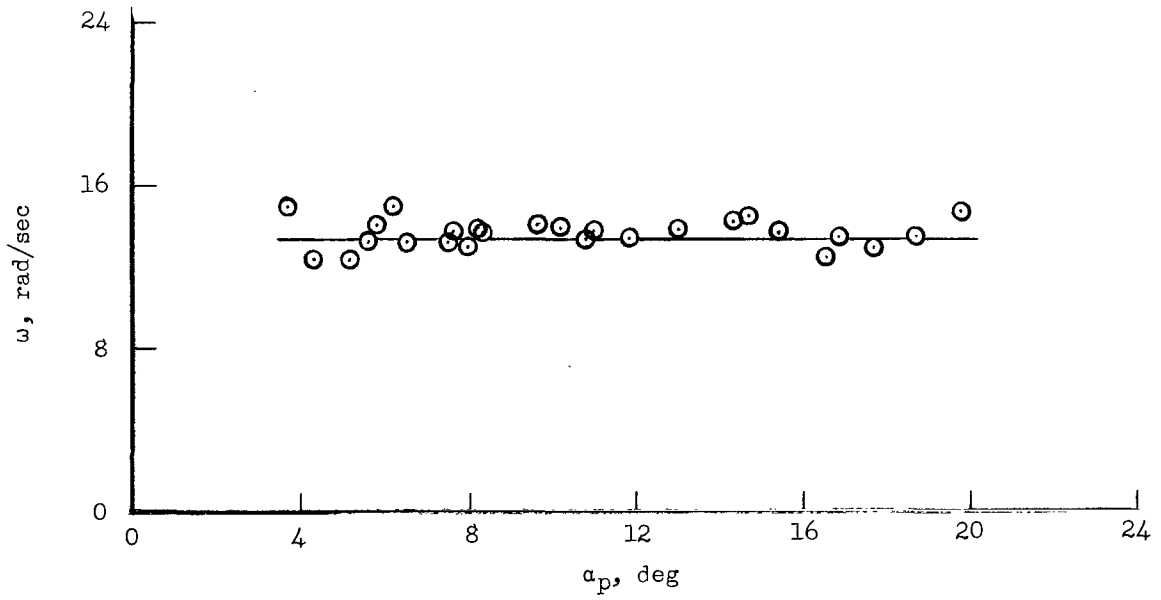
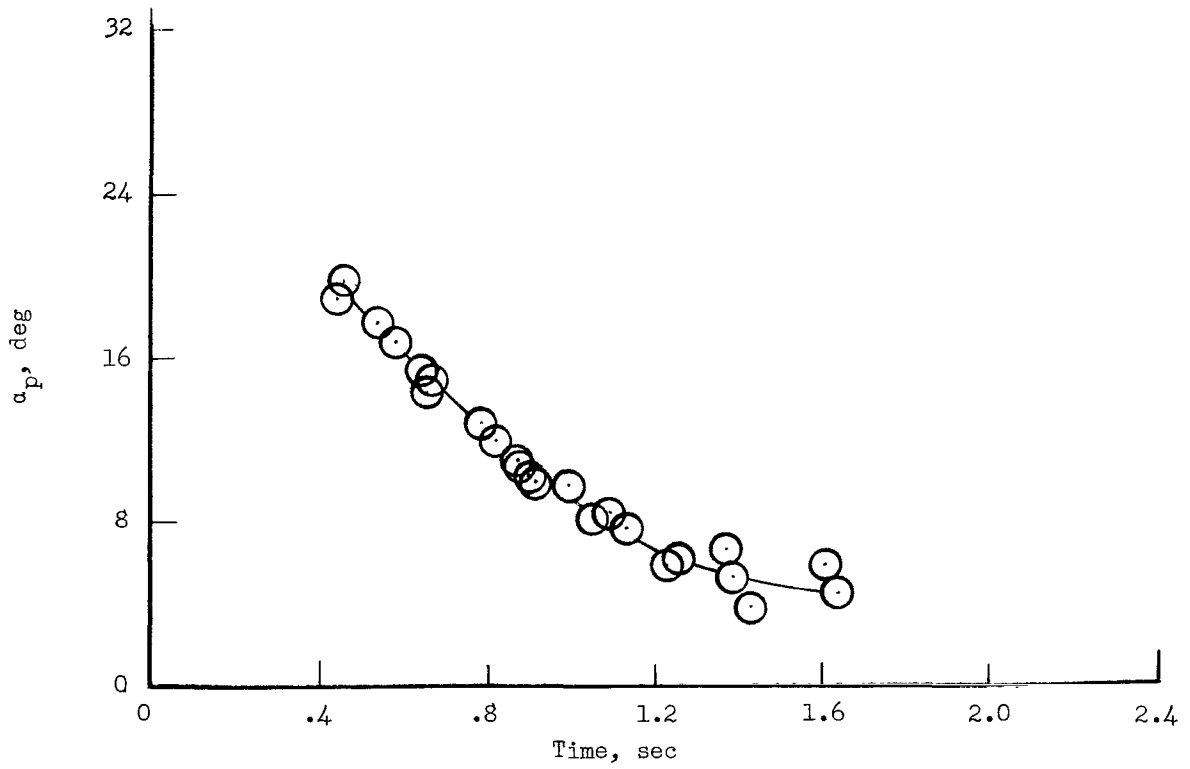
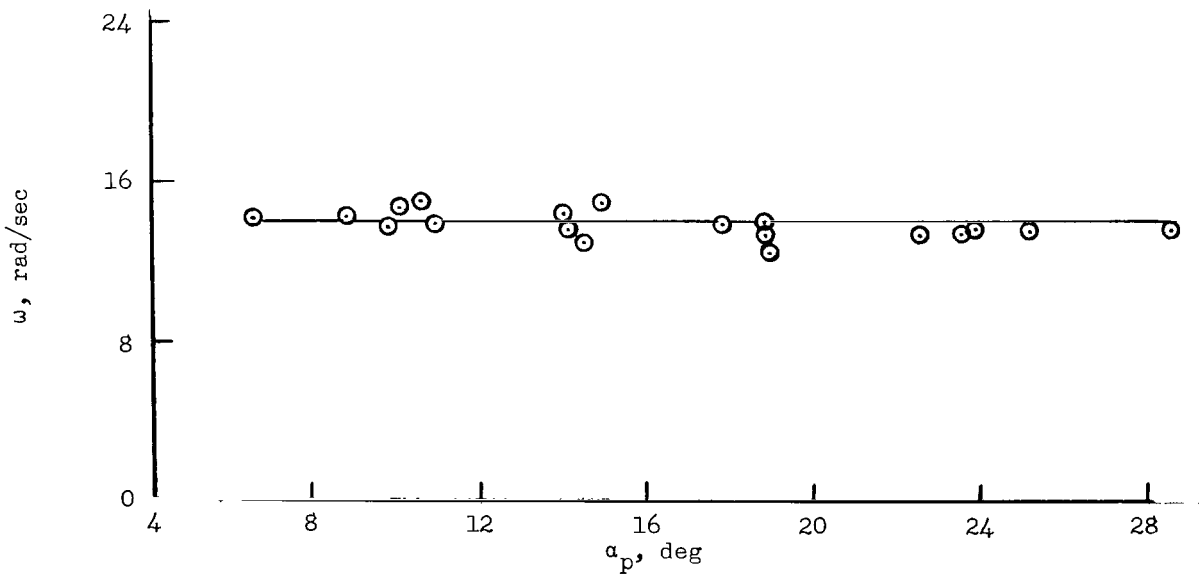
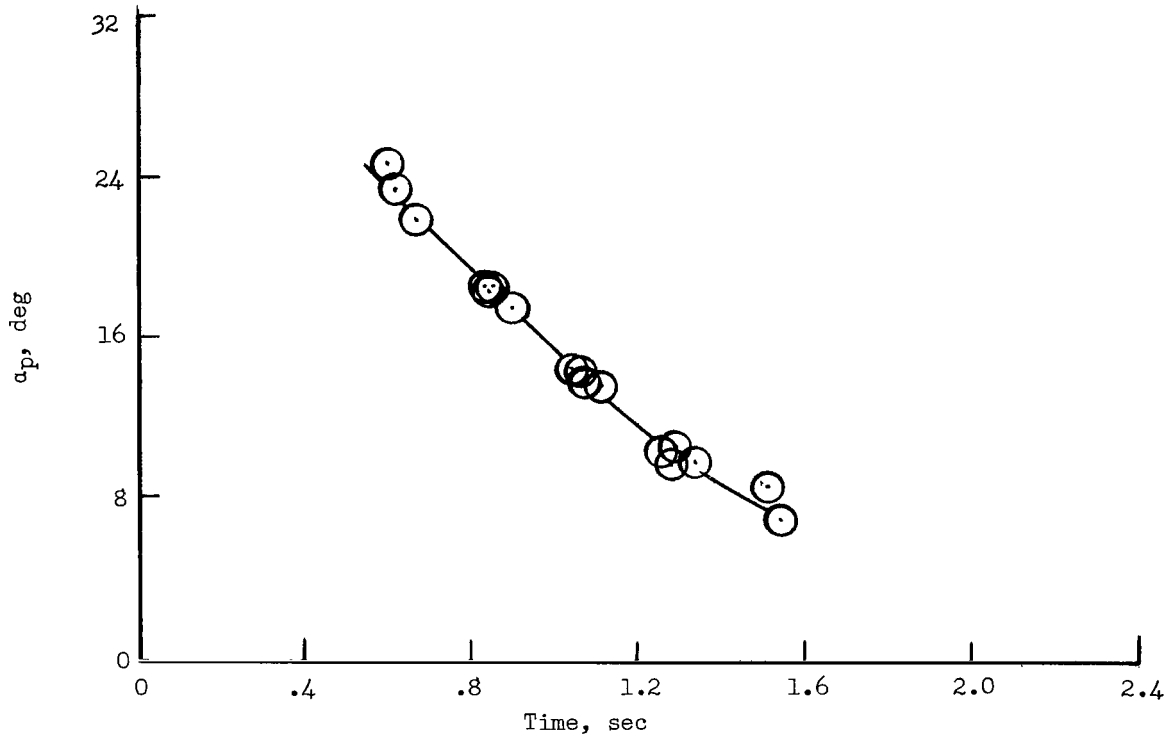


Figure 4.- Sample of test showing raw data, envelope fairing, and trim angle of attack.



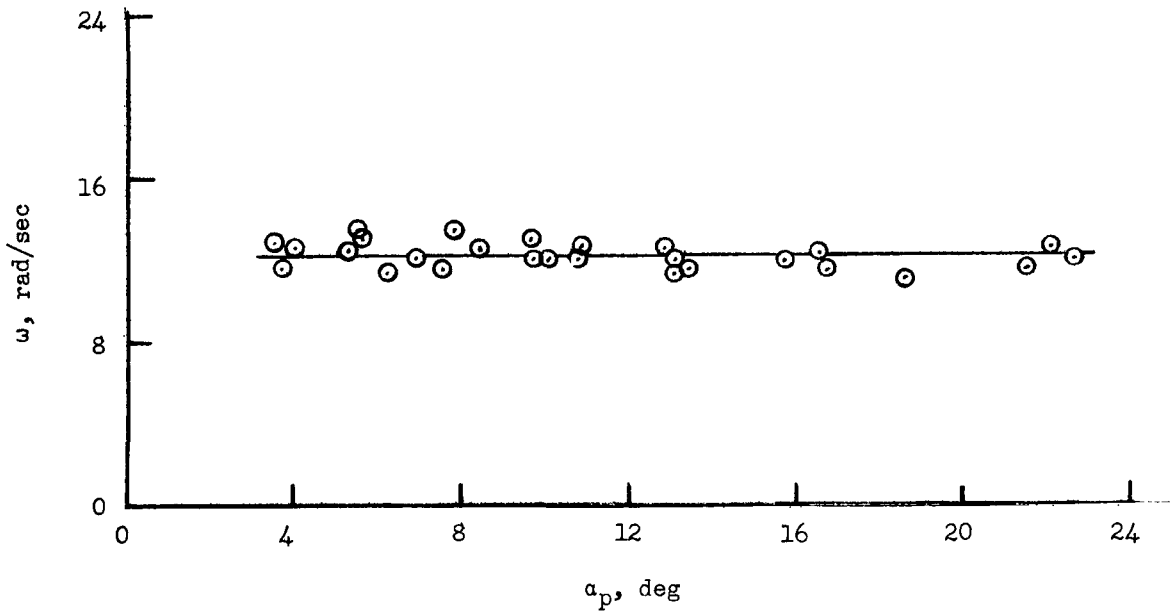
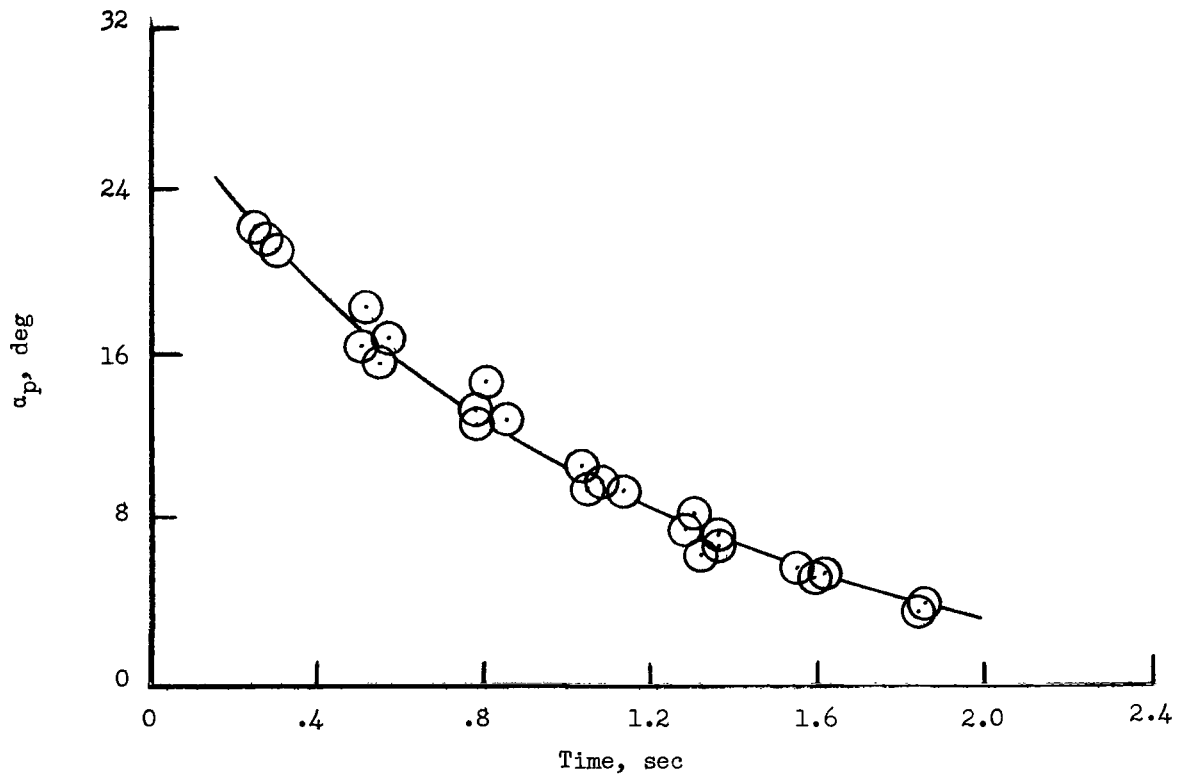
(a) Model 1.

Figure 5.- Angle-of-attack envelope and oscillation frequency.



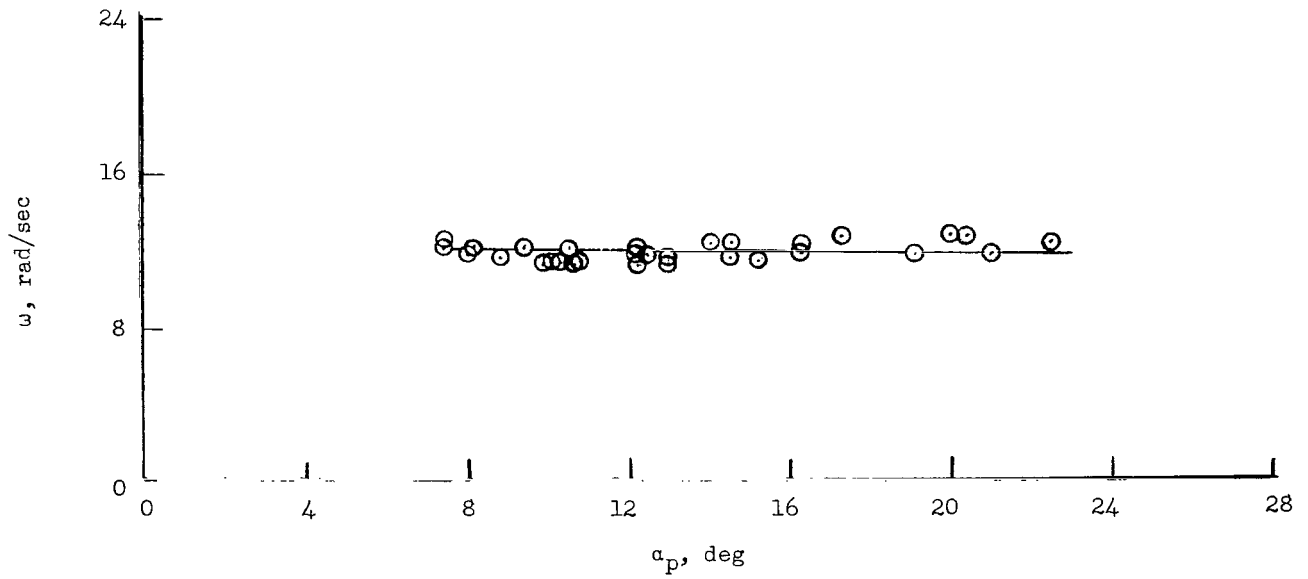
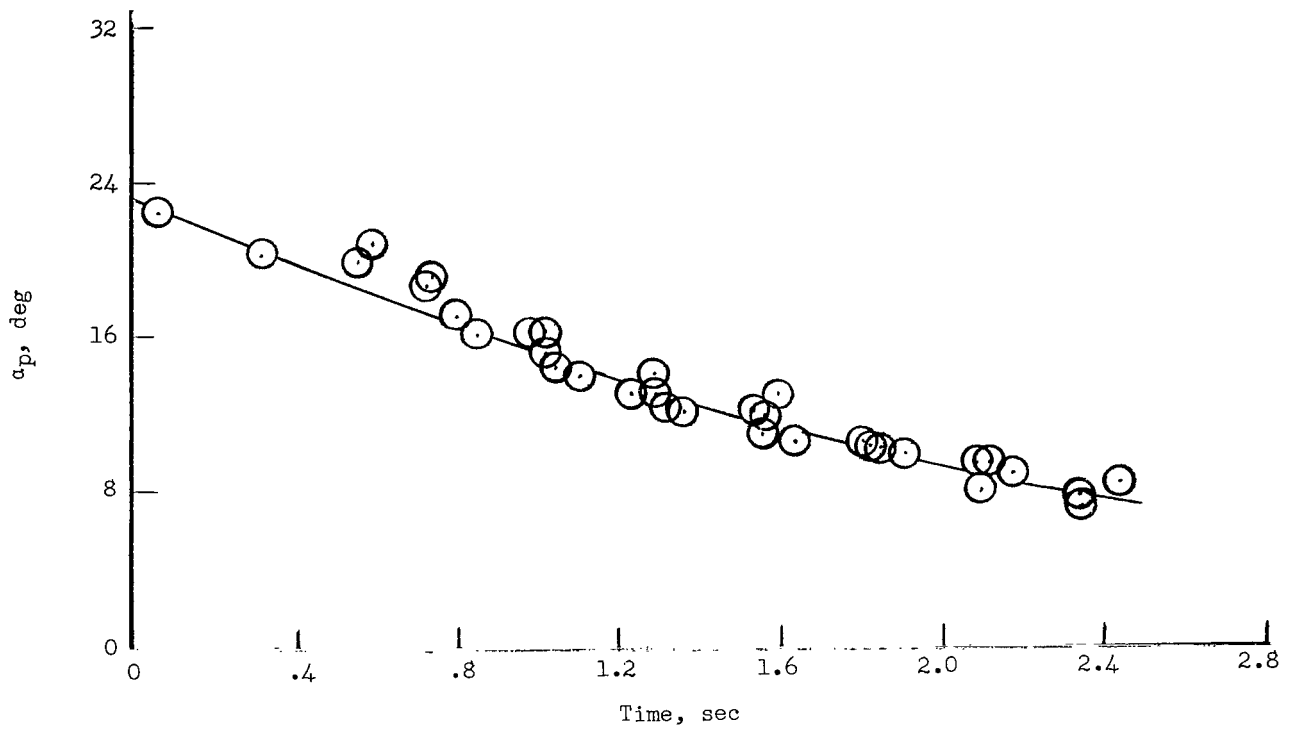
(b) Model 2.

Figure 5.- Continued.



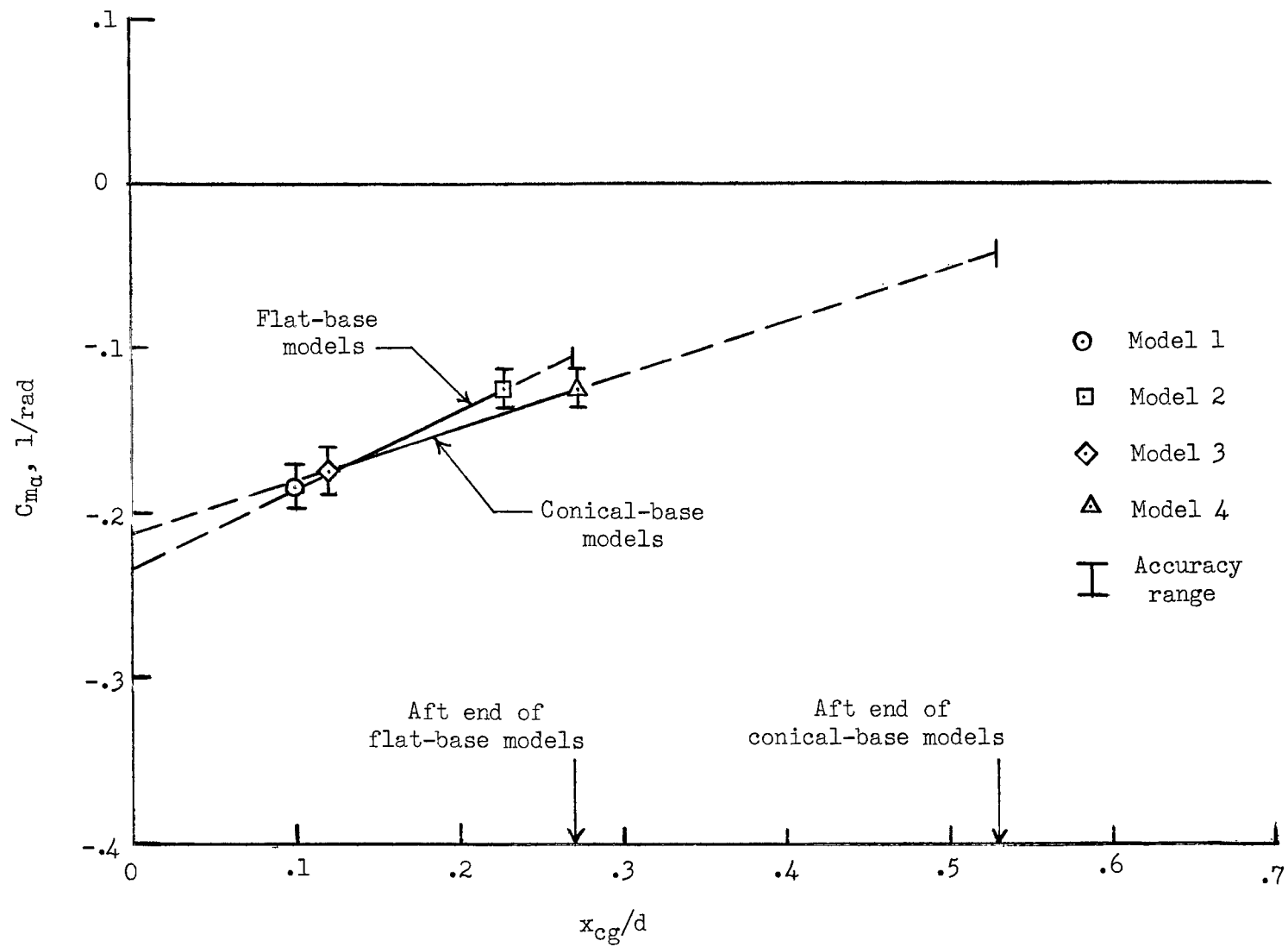
(c) Model 3.

Figure 5.- Continued.



(d) Model 4.

Figure 5.- Concluded.

Figure 6.- Variation of  $C_{m\alpha}$  with  $x_{cg}/d$ .

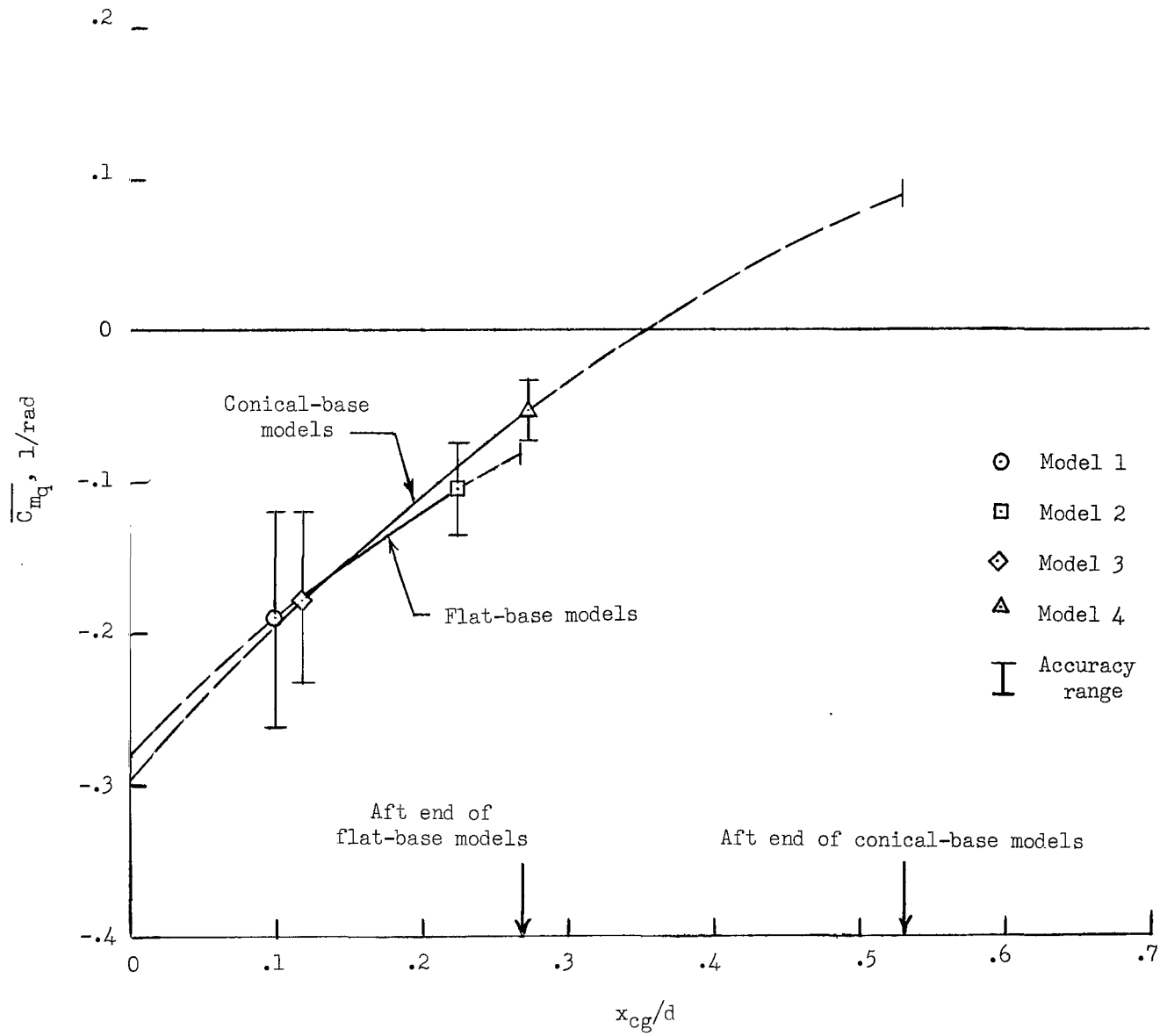


Figure 7.- Variation of  $\overline{C_{m_q}}$  with  $x_{CG}/d$ .

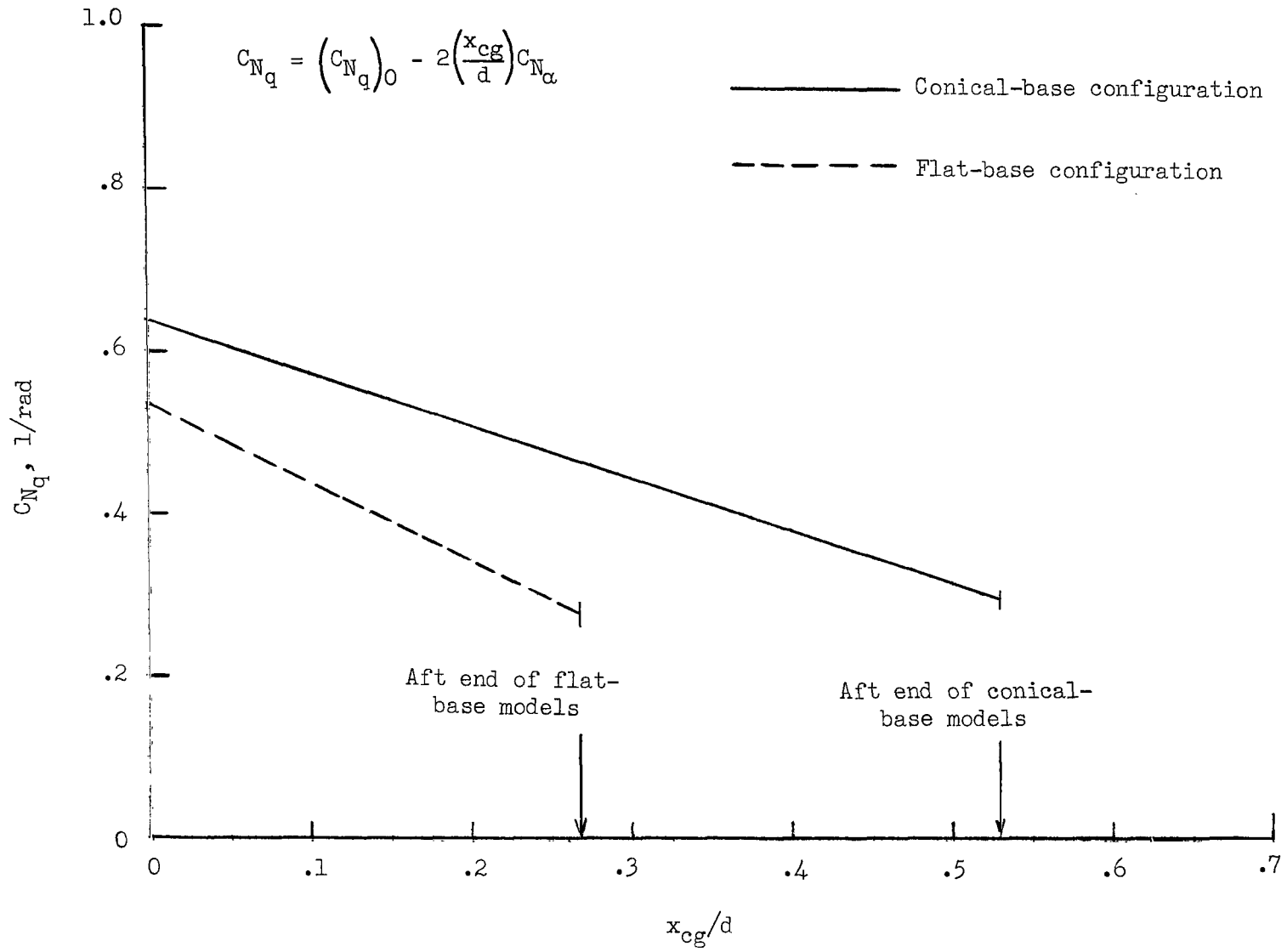


Figure 8.- Variation of  $C_{Nq}$  with  $x_{cg}/d$ .

*"The aeronautical and space activities of the United States shall be conducted so as to contribute . . . to the expansion of human knowledge of phenomena in the atmosphere and space. The Administration shall provide for the widest practicable and appropriate dissemination of information concerning its activities and the results thereof."*

—NATIONAL AERONAUTICS AND SPACE ACT OF 1958

## NASA SCIENTIFIC AND TECHNICAL PUBLICATIONS

**TECHNICAL REPORTS:** Scientific and technical information considered important, complete, and a lasting contribution to existing knowledge.

**TECHNICAL NOTES:** Information less broad in scope but nevertheless of importance as a contribution to existing knowledge.

**TECHNICAL MEMORANDUMS:** Information receiving limited distribution because of preliminary data, security classification, or other reasons.

**CONTRACTOR REPORTS:** Technical information generated in connection with a NASA contract or grant and released under NASA auspices.

**TECHNICAL TRANSLATIONS:** Information published in a foreign language considered to merit NASA distribution in English.

**TECHNICAL REPRINTS:** Information derived from NASA activities and initially published in the form of journal articles.

**SPECIAL PUBLICATIONS:** Information derived from or of value to NASA activities but not necessarily reporting the results of individual NASA-programmed scientific efforts. Publications include conference proceedings, monographs, data compilations, handbooks, sourcebooks, and special bibliographies.

*Details on the availability of these publications may be obtained from:*

SCIENTIFIC AND TECHNICAL INFORMATION DIVISION  
NATIONAL AERONAUTICS AND SPACE ADMINISTRATION  
Washington, D.C. 20546